Final Technical Report

USGS NEHRP AWARDS G15AP00085 & G15AP00088

^{10}Be Terrestrial Cosmogenic Nuclide Dating for Determining Slip Rates of Normal Faults in the Lake Tahoe Basin Collaborative Research with University of Nevada, Reno and University of Cincinnati, Ohio

Steven G. Wesnousky

Center for Neotectonic Studies, University of Nevada, Reno, 1664 North Virginia Street, Reno, NV 89557

Email: wesnousky@unr.edu

Tel: 775 784 6067

Lewis Owen

Dept of Geology, University of Cincinnati, PO Box 210013, OH 45221

Email: owenls@ucmail.uc.edu

Tel.513 556 6931

Start Date: 09/01/2015

End Date: 08/13/2016

Abstract

The West Tahoe Fault is the 45 km long, primary range-bounding fault of the Sierra Nevada at the latitude of Lake Tahoe, California. It is a N-NW striking, east dipping normal fault that has a pronounced terrestrial Holocene scarp extending from near Meyers, CA to Emerald Bay, where it continues offshore along the western margin of the lake until it approaches Tahoe City. The West Tahoe Fault displaces late Pleistocene moraines and glacial deposits along much of its extent. Terrestrial Cosmogenic Nuclide (TCN) surface exposure ages of sixteen boulders were collected from faulted moraines at Cascade Lake. Eight ages from the last-glacial Tioga moraine range from 13.9 to 23.4 ka, and seven of those ages average 21.2 ± 1.2 ka, similar to Tioga moraines elsewhere in the Sierra Nevada. The eight ages from the penultimate Tahoe moraine are scattered from 14.5 to 120.5 ka. Treatment of the oldest measured age of 120.5 ± 11.5 ka as the minimum age of deposition of the older Tahoe moraine is based on the assumption that morainal boulders contain little cosmogenic inheritance and scatter is largely the result of boulder surface erosion and exhumation, as well as the conclusions of other glacial studies regarding the ~140 ka timing of the Tahoe glaciation elsewhere in the Sierra Nevada. Vertical displacements measured from lidar on the crests of the Tioga and Tahoe moraines are 32 ± 12 and 59 ± 10 m, respectively. Dividing these displacements by the ages of the moraines, gives maximum vertical separation rates of 1.5 ± 0.7 and 0.5 ± 0.1 mm/yr since emplacement of the Tioga and Tahoe moraines respectively. At face value this implies a rapid increase in slip rate with time, but because nowhere else in this region is found evidence for rapid changes in slip-rates during the late Pleistocene, and as the post-Tahoe rate is more similar to previous estimates, it is suspected that this post-Tioga rate is an apparent rather than real rate, and is likely an artifact of morainal deposition over a pre-existing fault scarp. Dividing the post-Tahoe vertical separation rate by the sine of dips ranging from 50° to 70° results in a slip rate of 0.6 ± 0.2 mm/yr. Dividing an average surface slip of 1.3 m (based on the empirical relation between fault length and coseismic surface slip in Wesnousky, 2008) by this slip rate allows for an average return time for ~M7 earthquakes of ~2-4 ka on the West Tahoe Fault.

Introduction

The West Tahoe Fault is located along the western margin of the Lake Tahoe Basin in Northern California (Figure 1). It is a N-NW striking, east dipping normal fault that has a pronounced terrestrial Holocene scarp that cuts late Pleistocene glacial moraines and extends from near Meyers, CA to Emerald Bay (Figure 2), where it continues northward offshore along the western margin of the lake until it approaches Tahoe City. It is the westernmost fault of the Walker Lane at its latitude (38.7°- 39.3° N).

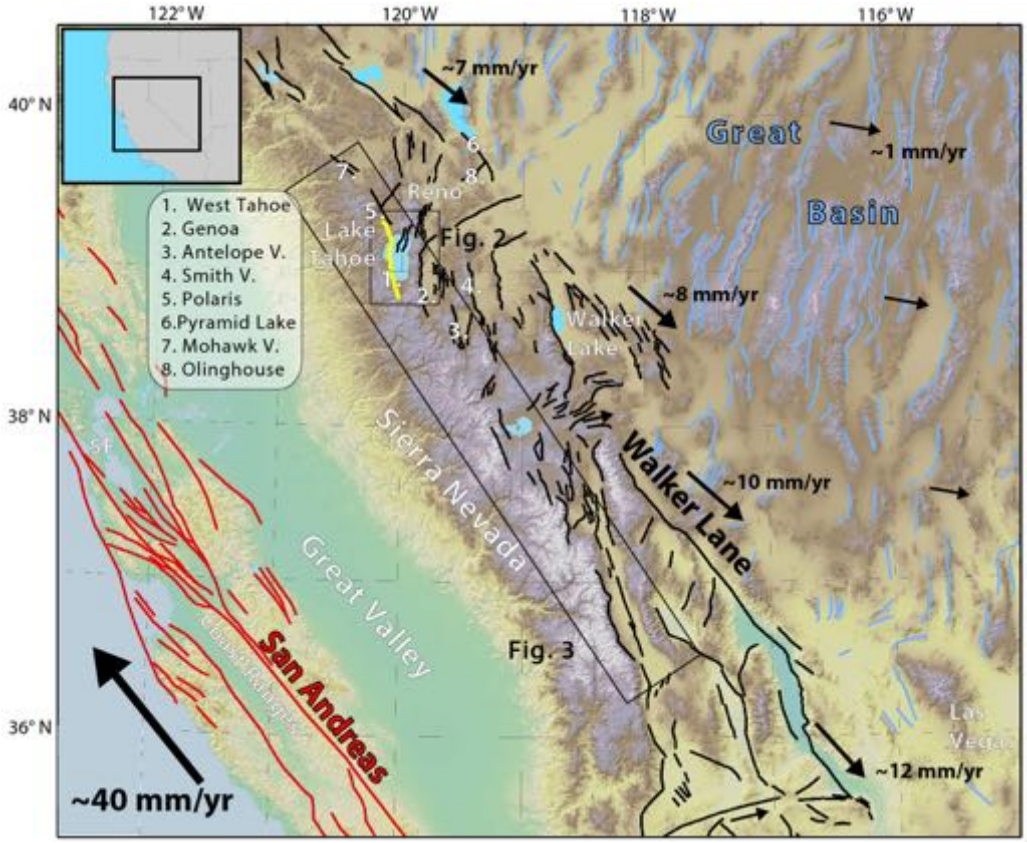

Figure 1 Overview map of the Walker Lane. The West Tahoe fault is shown as a thick yellow line and is part of the Walker Lane fault system (Black lines). Major faults of the Northern Walker Lane discussed in the text are numbered. Faults of the San Andreas system are shown in red and those of the Basin and Range in light blue. Black arrows are diagrammatic of GPS velocities relative to the Sierra Nevada. Faults are simplified from the USGS Quaternary Fault and Fold Database.

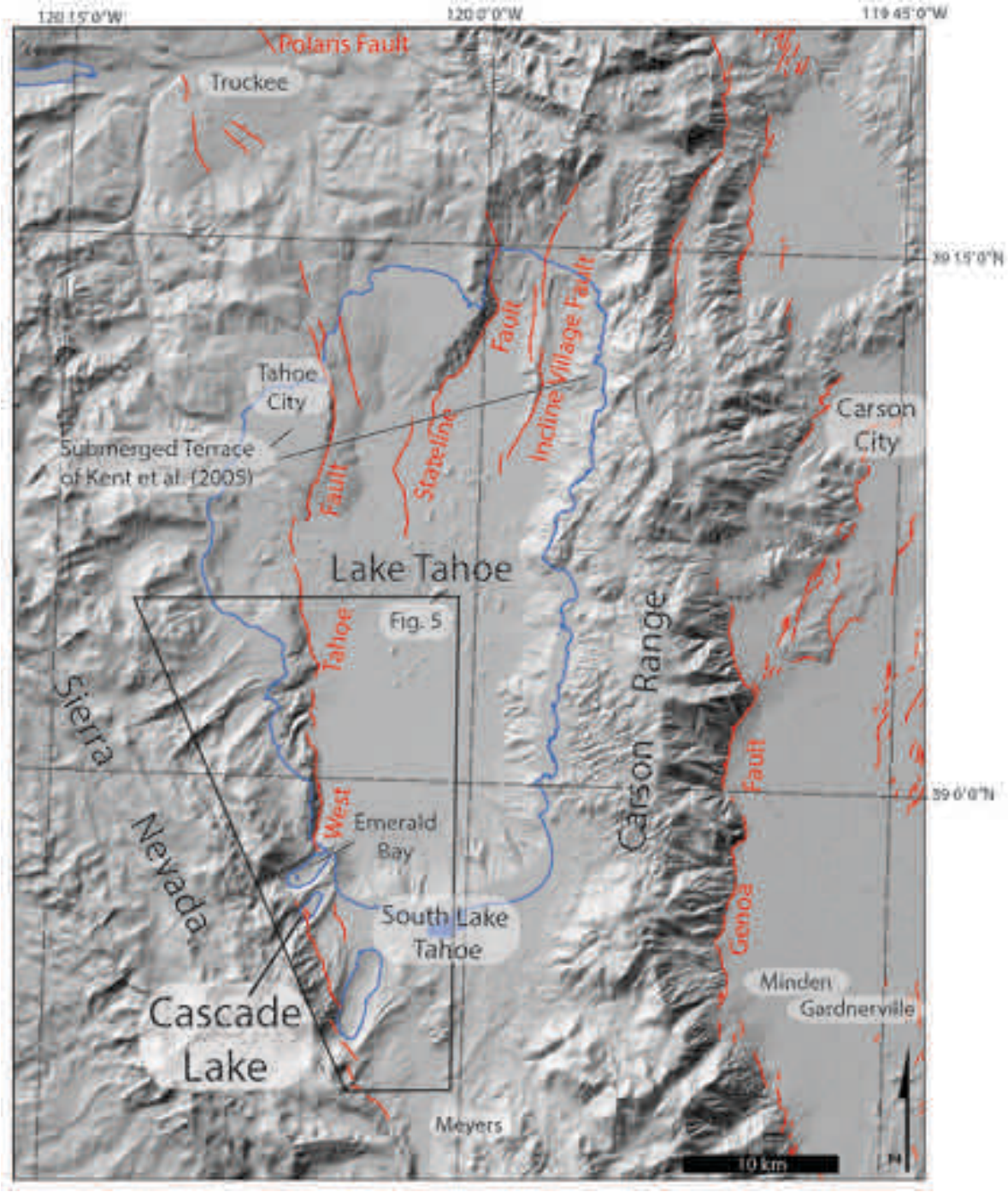

Figure 2 Hillshade of the Tahoe Basin and surrounding area. Lidar and bathymetric data are overlain over a 10 m hillshade. The shorelines of Lake Tahoe and other lakes are in blue. Major faults are in red. The submerged terrace that Kent et al. (2005) used to obtain a vertical separation rate of 0.5-0.75 mm/yr across the basin is indicated here.

We report here Terrestrial Cosmogenic Nuclide (TCN) ^{10}Be surface exposure ages (e.g. Gosse and Phillips, 2001) for 16 boulder samples collected from the surface of faulted moraines that bound the south side of Cascade Lake (Figure 2). The ages determined provide a basis to place limits on the timing of glaciation in the Tahoe Basin and assess the Late Pleistocene slip rate of the West Tahoe fault. We first provide an overview of both the history of glacial studies in the Sierra Nevada and the uncertainties in TCN exposure ages of glacial moraines. Next we will discuss prior studies of active faults in the vicinity of Lake Tahoe. we then describe the methods used for mapping, boulder sampling, and analysis. This is followed by presentation of the analytical results of the TCN dating and the uncertainties inherent within. The following section describes our slip rate calculations and the attendant uncertainties. The thesis concludes with a discussion that places the age results in the context of past glacial and fault slip rate studies and how these might relate to seismic hazard. The purpose of this thesis is to present new age data that allow for a better understanding of the timing of glaciations in the Tahoe Basin, and offer new constraints on the rate of slip for the West Tahoe Fault. This report is currently being edited for submission and publication and dissemination in a professional journal and is largely the Master thesis of Ian Pierce

Background

History of glacial studies in the Sierra Nevada

The Pleistocene glaciations of the Sierra Nevada have been studied for over a century, beginning with John Muir and Josiah Whitney who first described the glacially sculpted landscape in the late 19th century (Gillespie and Clark, 2011). The summaries of Fullerton (1986) and Gillespie and Clark (2011) provide a modern understanding of glacial chronologies in the Sierra Nevada, and are here summarized. The locations of prior studies of glacial chronology along the east flank of the Sierra Nevada are shown in Figure 3.

Blackwelder (1931) was among the first to study glacial deposits throughout the Sierra Nevada and focused much of his attention on the eastern slope. His and similar early efforts (e.g. Birkeland, 1964; Birman, 1964; Blackwelder, 1931; Clark, 1967; Putnam, 1960, 1949; Sharp, 1972; Sharp and Birman, 1963) found that at most drainages of the Eastern Sierra there were two or more sets of moraines that could be differentiated and correlated between drainages based on their geomorphology, cross cutting relationships, and degree of weathering. Based on these cross-cutting relationships, they showed that older moraines are more deflated and broader crested compared to younger moraines, that the granitic boulders composing these older moraines are in a greater state of disintegration than those on younger moraines, that the frequency and clast size of granitic boulders on these older deposits are less, while the remaining boulders are more ragged, and that the soil developed on younger tills is an ashen gray and reddish in older deposits. Direct comparisons of these degrees of weathering between different moraines allowed for a determination of relative age, and Blackwelder (1931) first showed that these moraines were deposited during at least two distinct late-Pleistocene glacial stages: the younger Tioga and older Tahoe stages, separated by

some length of time. Burke and Birkeland (1979) later developed methods for differentiating glacial moraines using soil development, and Gillespie (1982) pioneered a clast-sound-velocity technique that was able to determine the relative degree of weathering of boulders in morainal deposits. Early attempts at determining quantitative ages for these glaciations in the Sierra Nevada were limited to locations where glacial deposits are stratigraphically bound by volcanic deposits (e.g. Sawmill Canyon and June Lake, Figure 3) that could be numerically dated using radiometric Ar-Ar or K-Ar methods (Bursik and Gillespie, 1993; Dalrymple et al., 1982; Gillespie, 1982), or by use of proxies such as the global marine oxygen isotope record (Figure 4).

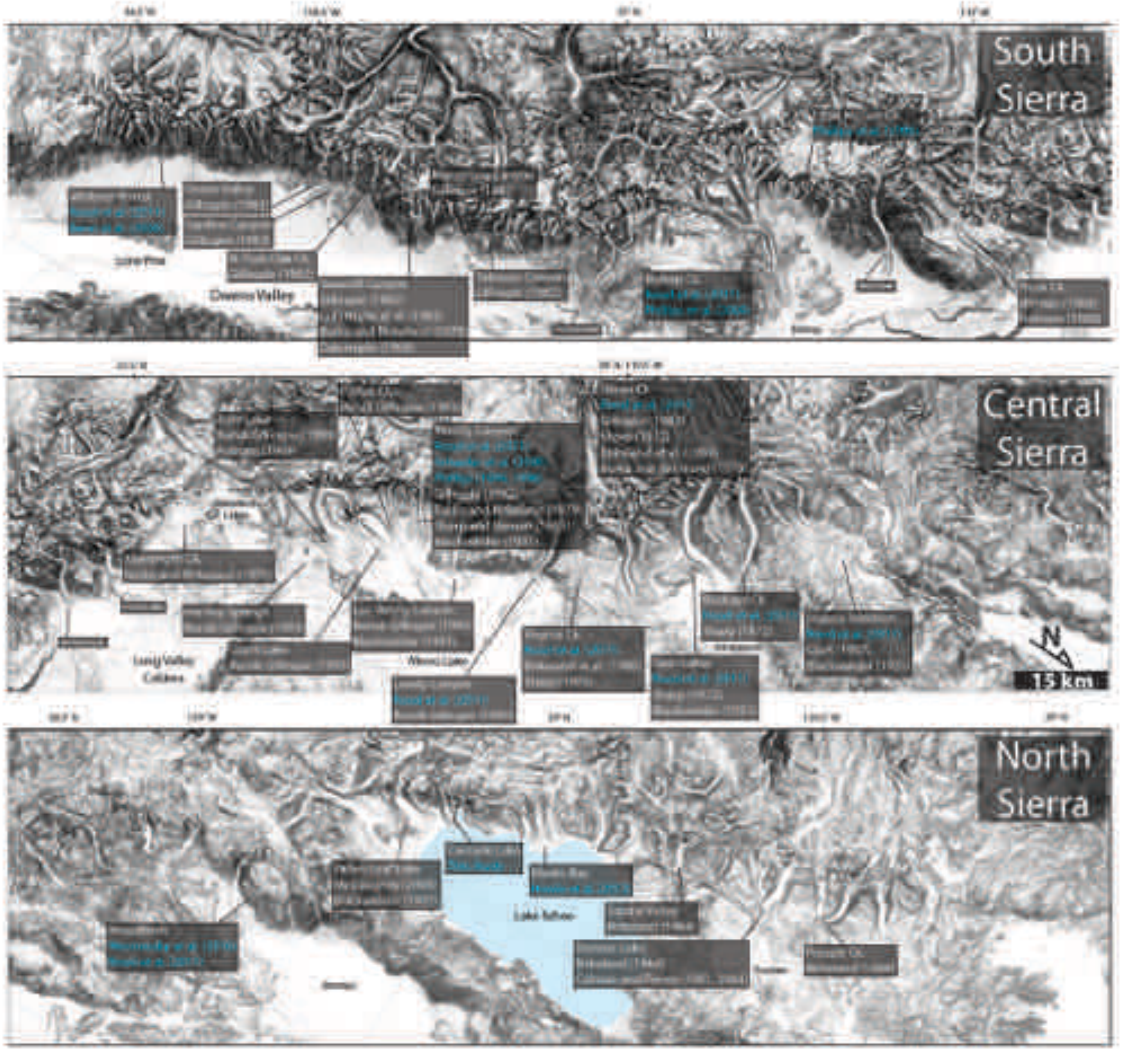

Figure 3 Slope shade images of the eastern flank of the Sierra Nevada showing locations and citations of previous studies of late Pleistocene glacial moraines and outwash deposits. Citations in blue text use cosmogenic nuclides to establish the numerical (vs. relative) ages of glacial deposits.

Deep sea sediment cores record a global climate record based on the ratio of ^{18}O to ^{16}O found in foraminifera (e.g. Pisias et al., 1984). This record is based on the premise that lighter water enriched with ^{16}O is preferentially stored in glacial ice, depleting ^{16}O in seawater as ice sheets reached their maxima. Thus the foraminifera in these cores with lower ratios of ^{18}O to ^{16}O suggest that when they were deposited seawater temperatures were warmer, less water was stored in glaciers, and there was a warmer climate, while higher ratios of ^{18}O to ^{16}O indicate the converse: more water was stored in continental ice sheets, and both the oceans and global climate were cooler. This climate record has been refined and calibrated with assumptions about orbital mechanics (i.e. Milankovitch cycles) (e.g. Martinson et al., 1987), and glaciologists have used it as a proxy for the timing of glacial ice. The marine oxygen isotope record has been broken into marine isotope stages (MIS) of prolonged warm or cool periods (e.g. Pisias et al., 1984) (Figure 4), with stages 2, 4, and 6 cool, and stages 1 and 5 warm. Sierran glacial advances have been correlated with these cool stages (e.g. Gillespie, 1991). In context for this study, the Tioga glaciation is generally correlated with MIS 2 (Figure 4) (Gillespie and Clark, 2011; Rood et al., 2011a). Similarly, the Tahoe glaciations referred to as Tahoe I and II correlate with MIS 6 (Rood et al., 2011a; Gillespie and Clark, 2011; Gillespie, 1991; Phillips et al., 2009, 1990) and MIS 4 (Gillespie, 1991; Gillespie and Clark, 2011; Phillips et al., 1996, 1990), respectively.

By the 1990's, relative dating studies and the marine oxygen isotope record had been used to assign relative and some numeric ages to moraines spanning the Eastern Sierra. The sum of these results led to a generally agreed upon sequence and naming of glacial stages. The names given to each advance, given in order of increasing age, were the Tioga, Tenaya, Tahoe II, Mono Basin, Tahoe I, and Sherwin stages of glaciation (Gillespie and Clark, 2011) (Figure 4- Sherwin is omitted, see figure caption). Generally, throughout the Sierra, Tahoe age moraines are generally quite large compared with Tioga deposits, and thus it is thought that the Tahoe glaciation was more extensive and larger than the Tioga glaciation (Gillespie and Clark, 2011).

With the advent of TCN exposure aging techniques (e.g. Gosse and Phillips, 2001), Phillips et al. (1990) were the first to directly measure the exposure age of glacial deposits in the Sierra Nevada at Bloody Canyon (center panel of Figure 3). The results of their mapping and analysis suggest that the moraine complex at Bloody Canyon was deposited during 5 distinct glacial stages: an older Tahoe (207 ka), Mono Basin (103 ka), younger Tahoe (59.8 ka), Tenaya (24.3 ka), and Tioga (21.4 ka) (Figure 4). The younger Tahoe and Tenaya moraines here are double crested, not dissimilar to many of the moraines in the Tahoe basin (Figure 5). These results have been contentious as there is an apparent cross cutting relationship where the younger (as dated) Mono Basin moraines appear to be cut by the older Tahoe right-lateral moraine, implying that the older Tahoe moraine should be younger than the Mono Basin moraine (Figure 1 in Phillips et al., 1990). This cross cutting relationship contradicts their results. Since then no known studies have re-dated these older moraines at Bloody Canyon to resolve this problem, but this apparent conflict can likely be explained by uncertainties in cosmogenic results that are discussed later in this section, where cosmogenic ages from older deposits are often highly scattered due to uncertainties in the post-depositional histories of boulders (e.g. Bierman and Gillespie, 1991).

The assignment of cosmogenically dated moraines to cool stages of the oxygen-isotope record is not perfect. For example, the study of Phillips et al. (1990) at Bloody Canyon (Figure 3) correlates the Mono Basin stage of glaciation to warm MIS 5 (Figure 4). As well, Rood et al. (2011a) suggest from their study that there was no major glacial advance during the cooler MIS 4. Thus, there remains uncertainty in the quantitative assignment of ages of glacial advances along the east flank of the Sierra Nevada and the relationship of the advances to the marine oxygen isotope record. Correlations of older glacial deposits are yet more tenuous, as the uncertainty of the ages of deposits increases while the resolution of the MIS record decreases (Gillespie and Clark, 2011).

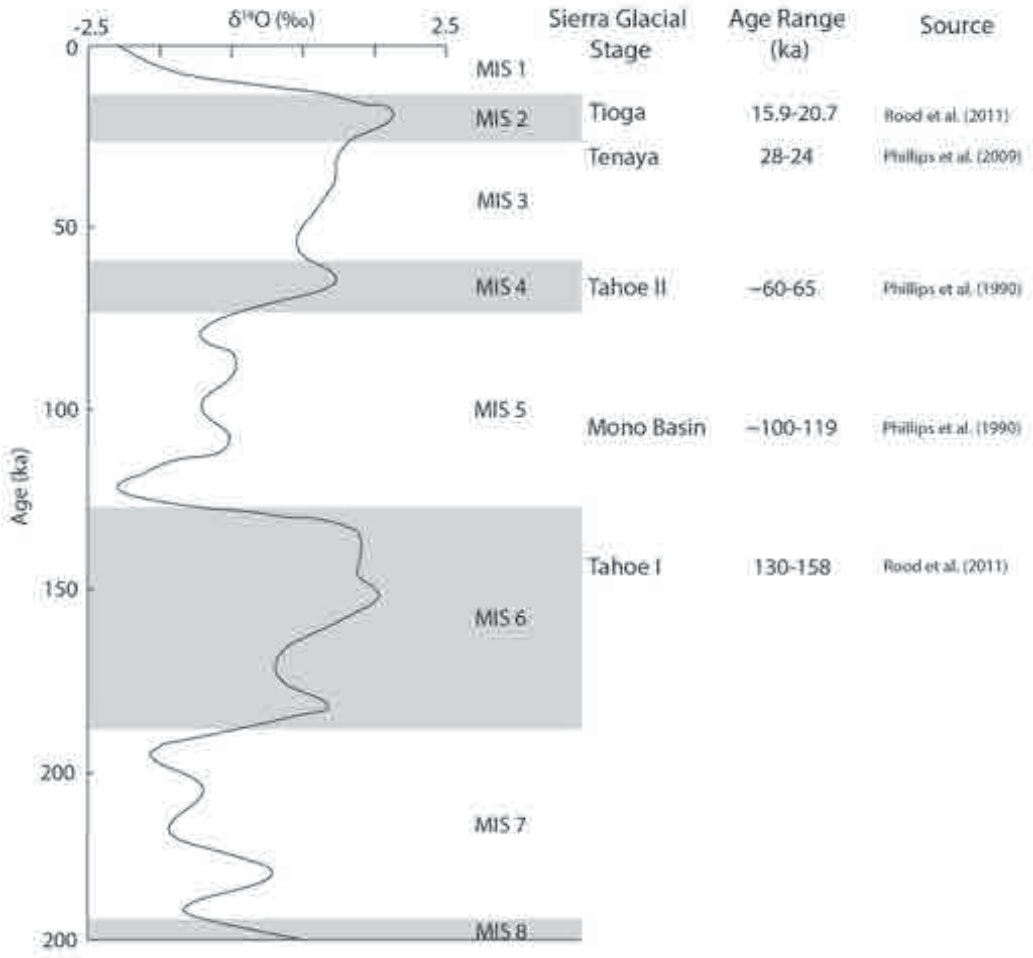

Figure 4 Chronology of Late Pleistocene glaciations, their ages, and the stages of the Marine Oxygen Isotope record. Modified from Gillespie and Clark et al. (2011). The Sherwin glaciation occurred before the Bishop Tuff, ~760 ka, so is omitted for simplicity.

Rood et al. (2011a) compiled 229 new and existing cosmogenic ages from glacial deposits in the central and southern Sierra Nevada (blue text in Figure 3), to show that the last glacial maximum (LGM), Tioga, reached its maximum during MIS 2 at 18.8 ± 1.9 ka, and that the penultimate glaciation (Tahoe I) retreated during MIS 6 at 144 ± 14 ka

(Rood et al., 2011a). They found no statistically significant ages for any of the other previously described glaciations intermediate to the Tioga and Tahoe stages (e.g. Tenaya, Tahoe II, Mono Basin) (e.g. Bursik and Gillespie, 1993; Gillespie, 1991; Phillips et al., 1996, 1990). Likewise (and included in the analysis of Rood et al. 2011a), the extensive results from Bishop Creek (Figure 3) (Phillips et al., 2009) also show this two stage glacial history, and there too is no evidence for intermediate, MIS 4 or 5 glaciations.

Both Rood et al. (2011a) and Phillips et al. (2009) report scatter in TCN results from Tahoe-age deposits in excess of 100 kyr. This scatter has largely been attributed to erosion, and is demonstrative of the need to collect large numbers of samples from these older deposits (e.g. Heyman et al., 2011; Phillips et al., 1990, 1996, 2009; Putkonen and O'Neal, 2006; Putkonen and Swanson, 2003; Rood et al., 2011a; Zreda et al., 1994). These problems do not seem to be as significant for the younger Tioga deposits, as the results are not as scattered (e.g. Rood et al., 2011a; many others), likely because less time has occurred for the weathering of boulders on young deposits, and because it is often possible to sample original, intact glacially polished surfaces on boulders from younger moraines (Putnam, *personal communication*). While it is possible for inheritance (prior exposure) to yield exposure ages that are older than the age of the deposit, it has been shown that for glacial deposits, it is generally unimportant due to the relatively rapid transport and proximal deposition (relative to their source) of the boulders comprising moraines (e.g. Heyman et al., 2011). The lack of inheritance in glacial deposits is demonstrated by the absence of old outlying ages in Tioga deposits (e.g. Rood et al., 2011a; Phillips et al., 2009; Benn et al., 2006; Schaefer, 2006).

The first type of erosion that can effect cosmogenic ages from morainal boulders is the progressive denudation of a moraine and the gradual exposure/exhumation of boulders. With time, moraines deflate as fine-grained morainal material is removed from the crest: this is apparent from the broad rounded crests of older moraines. This process exhumes previously shielded boulders, and progressively exposes them to cosmogenic rays (e.g. Phillips et al., 1996, 2009; Zreda et al., 1994). This can be mitigated to some degree by sampling the largest boulders exposed on the crest of moraines, as these boulders were most likely to be originally exposed (Zreda et al., 1994; Rood et al., 2011a). Computational models of moraine erosion (e.g. Putkonen and Swanson, 2003) have shown that for old moraines (e.g. Tahoe), with a sufficient sample size of 6-7 boulders, it is likely (>90%) that the oldest measured age is close to the actual age of the deposit, and thus we sampled 8 samples per surface and treat the oldest age sampled as a minimum age of deposition.

At the same time that moraines erode, the boulders composing the moraines also weather and erode, and geologically frequent forest fires can spall up to centimeters at a time off the surface of boulders (e.g. Bierman and Gillespie, 1991), which is enough to greatly reduce the apparent surface exposure ages of boulders. These processes do not affect all boulders uniformly, but do add uncertainty and scatter to the results that are not easily explained with a uniformly applied boulder surface erosion rate, and further imply that exposure ages from boulders on moraines should be treated as minima.

Rood et al. (2011a) ignore moraine denudation in their calculations, and focus on boulder erosion (e.g. spallation and weathering). They suggest that a maximum of 50 cm of surface denudation since Tahoe time (~3.6 m/Ma) is possible for glacial outwash deposits (not moraines) based on the results of a comparison of boulder heights with cosmogenic ages, where small boulders (<50 cm in height) give considerably less consistent results than boulders >50 cm in height. However, they suggest that 50 cm of boulder surface erosion over the last ~20-140 ka is unlikely based on the lack of field evidence for this degree of spallation, so instead use a preferred erosion rate of 0.6 m/Ma, based on the observed roughness of Tioga age boulders and previous studies of boulder erosion in the Sierra Nevada (e.g. Bierman and Gillespie, 1991). Rood et al. (2011a) also state that younger (Tioga) moraines are largely insensitive to variations in erosion rate, due to their relatively recent deposition.

Phillips et al. (2009) investigated the issue of the progressive exposure of boulders by calibrating a soil erosion model using sediment samples from the crest of moraines with an assumed moraine age. They used this model to determine soil erosion rates on the order of 25-37 m/Ma, which could result in 3.5-5.2 m of erosion from the crest of a moraine since the assumed MIS 6 moraine deposition age of 140 ka. This amount of erosion is sufficient to progressively expose even large boulders that were previously buried and shielded from cosmogenic rays. However, the initial depth of the boulder remains unknown unless an age of the moraine and an erosion rate are assumed, which to some degree defeats the purpose of measuring the ages of boulders using cosmogenics. This is likely why Phillips et al. (2009) also ignore moraine denudation in their calculations, and use a boulder erosion rate of 1.1 m/Ma, similar to that of Rood et al. (2011a). They do use moraine erosion to explain the scatter and apparent contradictions in some of their results.

As evident at Bloody Canyon (Phillips et al., 1990), and as Wesnousky et al. (2016) discuss, it is not uncommon to find younger boulder ages on moraines that must be significantly older than TCN ages suggest due to cross-cutting relations. In the Woodfords area south of Lake Tahoe (Figure 3), TCN results indicate moraines aged <60 ka bound >140 ka outwash (Wesnousky et al., 2016). This result is morphostratigraphically impossible as it implies that a younger moraine was deposited outside of the older outwash, while cross-cutting relations require that the bounding moraine was deposited before the outwash. These two examples demonstrate the importance of treating cosmogenic ages from glacial deposits as minimum ages of deposition.

Figure 5 shows the extent of major glacial deposits within the southwestern portion of the Lake Tahoe basin and the surface trace of the West Tahoe Fault. Tioga moraines are well expressed in all major valleys along the western margin of Lake Tahoe and form sharp crested lateral and terminal moraines (tan in Figure 5). An intermediate to Tioga and Tahoe deposit (light blue in Figure 5) is only found at Fallen Leaf Lake and is differentiated from Tioga deposits based on its displacement by a small fault scarp that does not cut the younger Tioga deposits, and is differentiated from the Tahoe moraines based on cross cutting relations. Where present, Tahoe moraines are larger and morphostratigraphically located outside of Tioga deposits (blue in Figure 5). Tahoe

crests are rounder and broader, and the best-preserved example of a Tahoe aged moraine near Lake Tahoe forms Angora Ridge at Fallen Leaf Lake (Figure 5, McCaughey, 2003). Pre-Tahoe deposits are rare, but where present form highly eroded morainal features near the ends of some of the morainal complexes (e.g. Saucedo, 2005).

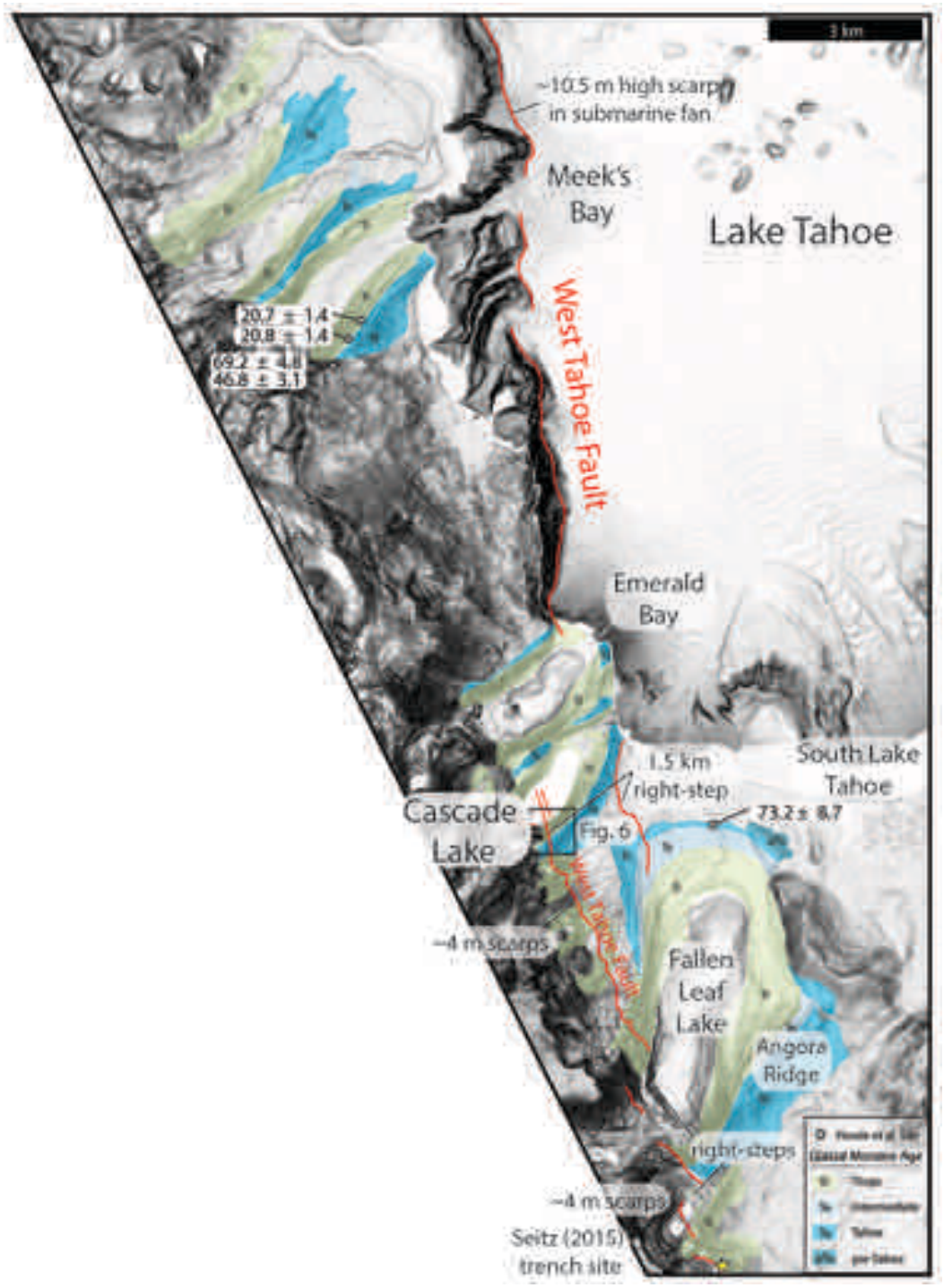

Figure 5 Extent of major late Pleistocene glacial deposits in the southwestern Tahoe Basin, trace of West Tahoe Fault (red), and annotations of notable features along fault strike. The basemap is a 0.5 m lidar and 10 m bathymetric derived slope-shade. The four cosmogenic ages near Meek's Bay, and the single OSL age near Fallen Leaf Lake are from Howle et al. (2012).

Near Meeks Bay in the Tahoe Basin, Howle et al. (2012) measured two ^{10}Be TCN ages from boulders on a Tioga moraine (Saucedo, 2005; Howle et al., 2012) resulting in ages of 20.8 ± 1.4 ka and 20.7 ± 1.4, and two boulders on a Tahoe moraine (Saucedo, 2005; Howle et al., 2012) resulting in ages of 46.8 ± 3.1 and 69.2 ± 4.8 ka (Figure 5). They also used an unpublished optically stimulated luminescence (OSL) age of 73.2 ± 8.7 ka, sampled from lake sediments below a Tahoe terminal moraine near Fallen Leaf Lake, to suggest that the Tahoe deposits near Lake Tahoe correlate with the ~60 ka MIS 4 Tahoe II deposits at Bloody Canyon of Phillips et al. (1990, 1996) (Figure 3).

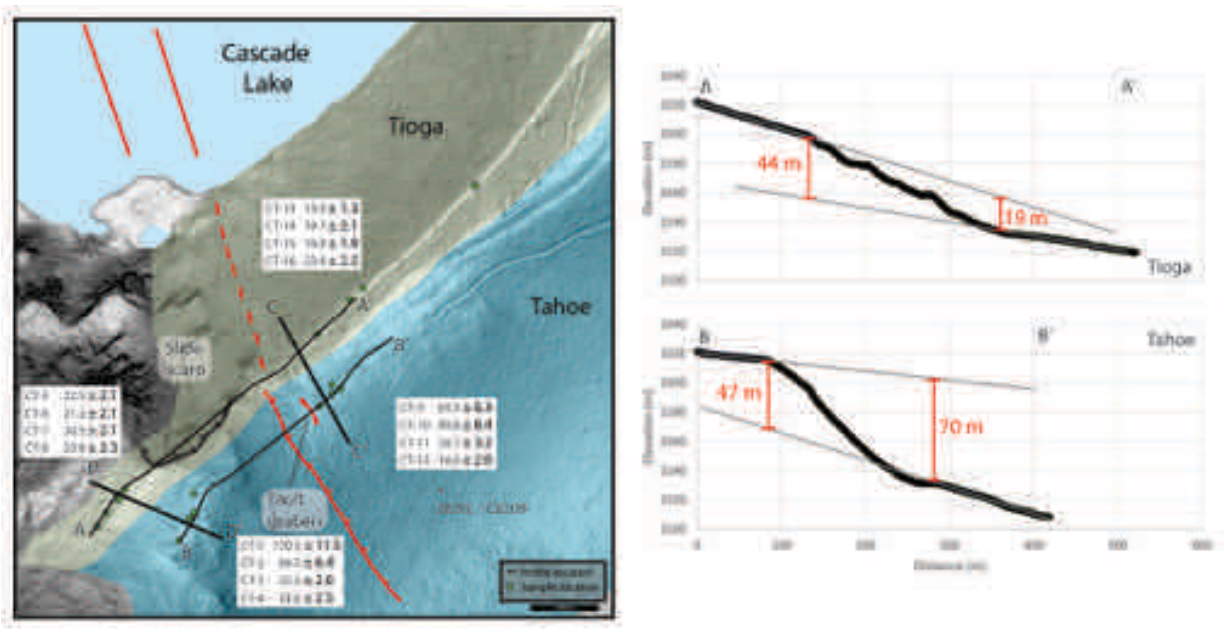

Figure 6 Detailed site map of the right lateral moraines at Cascade Lake where the West Tahoe Fault vertically displaces them. Cosmogenic ages (with 0.6 m/Ma erosion) and boulder sample locations are indicated by yellow dots. The Tahoe aged moraine is blue and Tioga aged is tan. Along moraine profiles A-A' and B-B' are shown to the right, and the locations of the profiles in Figure 7 are indicated by transects C-C' and D-D'. A lat/long coordinate for field reference is labeled in black.

Cascade Lake is a small lake dammed by glacial moraines on the southwestern edge of Lake Tahoe (Figure 5). Figure 6 shows where the West Tahoe Fault (red) cuts the right-lateral Tioga (tan) and Tahoe (blue) moraines at Cascade Lake, as well as the locations and results of my cosmogenic boulder samples. These moraines are primarily composed of granodiorite boulders sourced from the adjacent Sierra Nevada Mountains. Like Bloody Canyon (Figure 3), the right lateral moraine at Cascade Lake is a compound, double crested moraine complex composed of Tioga and Tahoe deposits. These

deposits are distinctly different: the outer, older Tahoe deposits form a much broader and rounder crest (Figure 7), composed of weathered boulders, while the younger Tioga crest is much narrower, sharper, and composed of less weathered boulders (Figure 7). On the hanging wall of the fault, these moraines exhibit an inverted topographic relationship: that is the inner, younger Tioga moraine is significantly higher than the outer, older Tahoe moraine (Figure 7). On the footwall, this relation is reversed: the outer Tahoe moraines are higher than the Tioga moraines (Figure 7), as is typical elsewhere in the Sierra Nevada (e.g. Gillespie and Clark, 2011), where Tahoe moraines are often considerably larger than Tioga moraines. This phenomenon of moraine height reversal across a fault has been attributed to active faulting in the past at Bloody Canyon and Pine, Parker, and McGee Creeks (Figure 3) (e.g. Birkeland and Burke, 1979).

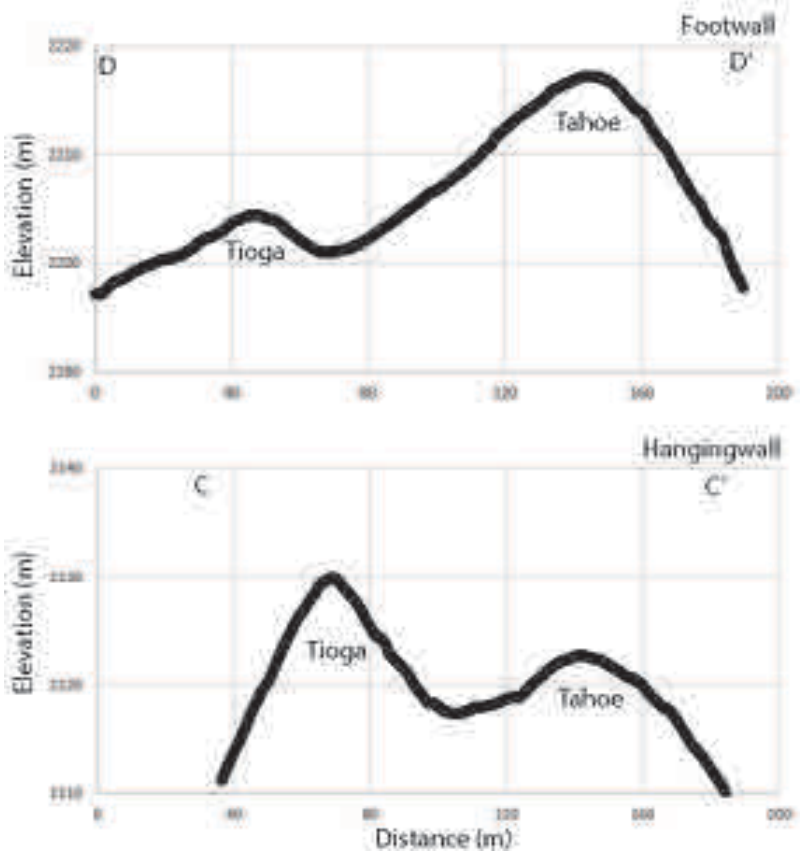

Figure 7 Cross moraine/fault parallel profiles at Cascade Lake showing the inverted relation of right lateral Tahoe and Tioga moraines across the fault. On the footwall (top), the Tahoe moraine is higher than the Tioga moraine and this relation is reversed on the down-dropped hanging wall (bottom). Elsewhere in the Sierras (Figure 3), Tahoe aged moraines are often considerably higher than those of Tioga age, more similar to that observed on the footwall here. The locations of these profiles are indicated on Figure 6.

Tectonic setting of the West Tahoe Fault in the Walker Lane

The Walker Lane is a 500 km long x 100 km wide northwest trending zone of discontinuous active faults and disrupted topography that accommodates up to 25% of the ~50 mm/yr of dextral shear between the Pacific and North American plates (Bennett et al., 2003; Dixon et al., 2000; Thatcher et al., 1999; Unruh et al., 2003). The Walker Lane sits between the semi-rigid block that makes up the Sierra Nevada mountains (Unruh et al., 2003) to the west and the north-northeast trending normal faults and ranges of the Great Basin to the east, roughly following the California-Nevada border from approximately the Garlock Fault in Southern California, northward past Lake Tahoe, CA (Figure 1). The Walker Lane is well defined geodetically by a zone of ~12 mm/yr of northwest directed right-lateral shear in the southern part, decreasing to ~8 mm/yr at the latitude of Lake Tahoe in the Northern Walker Lane (e.g. Bormann et al., 2016), while the San Andreas fault system accommodates ~40 mm/yr of dextral shear, west of the Sierra Nevada (e.g. Freymueller et al., 1999). Throughout the Walker-Lane, this shear is expressed as transtension that is accommodated in different ways: as oblique slip along well defined faults (e .g. Wesnousky, 2005), partitioned into normal faults at range fronts with separate strike-slip faults along the interiors of basins (e.g. Beanland and Clark, 1994), and other times is poorly located and understood to be taken up by distributed zones of discontinuous faults and larger scale block rotations (e.g. Wesnousky et al., 2012).

The half-graben holding Lake Tahoe (Figure 2) is part of the Northern Walker Lane, where dextral transtensional shear is accommodated in the absence of major through-going right-lateral strike-slip faults (Wesnousky et al., 2012). The West Tahoe Fault shares a similar strike, slip rate, and length as the eastward neighboring basins and normal faults: the Genoa, Smith Valley, and Antelope Valley Faults (Figure 1). To the north of Lake Tahoe, the shear detected by geodesy does appear to be accommodated by the optimally oriented Polaris, Mohawk, and Pyramid Lake strike-slip faults (Figure 1) (e.g. Angster et al., 2016; Gold et al., 2014; Hunter et al., 2011).

Lake Tahoe is bounded by the Sierra Nevada to the west (Figure 2), and thus the West Tahoe Fault forms the Sierra Nevada Frontal Fault at this latitude (38.7°- 39.3° N). The slip rate of the Sierra Nevada Frontal Fault increases southward, from 0.3 ± 0.1 mm/yr at Buckeye Creek and Sonora Junction (Figure 3) to 1.3 +0.6/ -0.3 mm/yr near Lundy Canyon (Rood et al., 2011b). Rood et al. (2011b) show that these slip rates have been relatively constant for the Sierra Nevada Frontal Fault Zone through Tioga and Tahoe time (i.e. the last ~150 ka). East of the West Tahoe Fault, there are two other faults in the Tahoe basin (Figure 2): the Stateline-North Tahoe Fault and the Incline Village Fault (Dingler et al., 2009). Both are primarily north-striking, east-dipping normal faults that lack a demonstrable shear component, in map view appear to form a general en-echelon right-stepping pattern (Figure 2), and are primarily subaqueous except for their northernmost portions.

The West Tahoe Fault is a 45 km long, N-NW striking, east dipping normal fault that has a pronounced terrestrial Holocene scarp extending from near Meyers, CA to Emerald

Bay (Figure 2). Two recognized strands of the West Tahoe Fault cut the onshore glacial deposits in the southwestern portion of the Tahoe basin (Figure 5).

The first, southern strand forms semi-continuous right-stepping, prominent, and youthful 3-5 m high east facing fault scarps that extend northwest from Meyers, California ~15 km towards Cascade Lake Figure 5. Seitz (2015) trenched the southern portion of this strand to the south of Fallen Leaf Lake (star on Figure 5) and found evidence for three Holocene earthquakes in the last 10 ka: 5.5 ka, ~7.2 ka, and ~9 ka, with vertical displacements of 1.4 m, 0.8 m, and 1.0 m, respectively. These are likely responsible for these observed youthful scarps (Seitz, 2015). At Cascade Lake, this fault cuts and progressively offsets the right lateral Tioga and Tahoe moraines with scarp heights of approximately 32 m and 59 m, respectively, before stepping eastward towards Fallen Leaf Lake.

The second, northern strand is ~30 km long, and forms a small fault scarp that vertically displaces the outermost terminal moraines (mapped Tenaya and Tahoe) at Fallen Leaf Lake. It then trends northward and offshore, around the terminal moraines of Cascade Lake, and into Lake Tahoe, where it has been imaged running north through the lake using high-resolution seismic chirp and acoustic-multibeam-derived bathymetry (Figure 2) (Brothers et al., 2009; Dingler et al., 2009; Kent et al., 2005; Maloney et al., 2013).

The southern segment, from Meyers to Cascade Lake, is generally northwest striking, whereas the northern, primarily offshore segment of the West Tahoe Fault is more northerly striking. Both of these segments contain frequent small right-steps and are somewhat sinuous. While nowhere along the fault are found measureable right-lateral displacements, this right stepping geometry might accommodate some amount of northwest directed right-lateral shear, as suggested by geodesy (e.g. Bormann et al., 2016).

Kent et al. (2005) estimate a vertical separation rate of ~0.5 mm/yr based on the ~10 m vertical displacement of a Tioga-aged paleo-shoreline terrace across the lake (Figure 2), and the ~30 m vertical displacement of Cave and Eagle Rocks, which they assume were wave modified ~60 ka, when the level of Lake Tahoe was raised by glacial damming of the Truckee River (e.g. Birkeland, 1968, 1964) during a presumed MIS 4 glaciation. Dingler et al. (2009) estimate a vertical separation rate for the West Tahoe Fault of 0.4-0.8 mm/yr based on the ~10.5 m displacement of an assumed Tioga-aged submerged fan delta (Figure 5) and the same displaced paleo-terrace as Kent et al. (2005). Howle et al. (2012) estimate a vertical separation rate for the onshore component of the West Tahoe Fault of 0.3 ± 0.1 mm/yr based on ~4 m vertical separation of ponded, post-Tioga (<14 ka) alluvium (Figure 5). None of these rates are constrained by numerical age data, and all rely on assumed ages and geomorphic relationships. Recent efforts using dense-network GPS driven geodetic block models to constrain the slip rates of faults in this part of the Walker Lane, suggest that the extension rate of the West Tahoe Fault is approximately 1.1 ± 0.4 mm/yr with 0.2 ± 0.4 mm/yr of right-lateral slip (Bormann et al., 2016; Hammond et al., 2011), considerably higher than these geologic estimates.

Howle et al. (2012) and Schweickert et al. (2004) have interpreted that the onshore component of the West Tahoe Fault is part of a larger “Tahoe-Sierra frontal fault zone,”

extending northward on land from near Cascade Lake, across Emerald Bay, and cutting the moraines near Meek's Bay shown in Figure 5. For simplicity this fault mapping is omitted from Figure 5, but is shown in Figure 2 of Howle et al. (2012). Many of the observations supporting the activity of the northern part of this fault zone are based on an older, lower quality lidar dataset, and when examined with the newer dataset used in this and other more recent studies, they appear to be primarily glacial ice stream breaches along moraine crests or slope failures (Seitz, 2015). Additionally there is no evidence for post-glacial faulting in the detailed seismic reflection profiles across where this fault zone has been mapped in Emerald Bay (Dingler et al., 2009), and the amount of slip assigned to this zone is in exceedance of the geodetically observed slip budget for the entire basin (e.g. Bormann et al., 2016), of which the three other well documented faults in the basin contribute to.

Methods

Mapping and scarp analysis

Moraines along the western shore of Lake Tahoe were analyzed and mapped using a combination of airborne imagery and lidar data (Watershed Sciences, 2011). To differentiate the relative age of glacial deposits, We used moraine morphology characteristics including: the height, width and sharpness of moraine crests (Figure 7), cross-cutting relations, and topographic position with respect to other moraines (e.g. outer moraines are older). Figure 5 is the result of my mapping and is generally in accord with previous interpretations (e.g. Howle et al., 2012; McCaughey, 2003; Saucedo, 2005; Seitz, 2015).

Topographic profiles are constructed using ArcGIS v10.3 with the 0.5 m/pixel Lake Tahoe lidar dataset (Watershed Sciences, 2011) along transects A-A' and B-B' (Figure 6), on the Tioga and Tahoe moraine crests, and on transects C-C' and D-D' (Figure 7), transverse to the moraine crests. A linear regression is fit to each moraine crest profile on both the hanging and footwalls of the fault (Figure 6). These regressions are then projected across the fault. Typical methods used for measuring the vertical separation rate by measuring the elevation difference between the parallel projections of the footwall and hanging wall surfaces (e.g. Swan et al., 1980) do not work here as the projections of these surfaces are not parallel, and when back-slipped the surfaces do not appear to match. Thus, minimum and maximum offsets are measured at the head and toe of each fault scarp (Figure 6).

Sampling and laboratory analysis

Sampling focused on the largest (>1 m in height) granitic boulders from each moraine crest as to limit the possibility of post-depositional transportation or exhumation/denudation (e.g. Owen et al., 2002), and to reduce the likelihood that the boulders were covered with snow for much of the year. Four boulders each were sampled from each of the following 4 surfaces of the right-lateral moraine complex at Cascade Lake (16 total boulders): from the Tioga moraine on both the foot and hanging walls of the West Tahoe Fault, and from the Tahoe moraine on both the foot and hanging walls of the West Tahoe Fault (Figure 6). Samples were taken from the tops of

these boulders to reduce any effects of exposure shielding (Gosse and Phillips, 2001). Photos of each boulder sampled are in Supplemental S1.

All sixteen samples were processed at the Cosmogenic Dating Preparation Laboratories at the University of Cincinnati following the methods of Kohl and Nishiizumi, 1992 (e.g. Owen et al., 2002; Rood et al., 2011a). Samples are first crushed and sieved to acquire the 250-500 μm size fraction. These are rinsed in recycled aqua regia to remove any organics or carbonates. Next, samples are etched in a 5% HF solution to remove meteoric Be as well as anything else that readily dissolves in HF. The samples are run through a Frantz magnetic separator to remove magnetic minerals. Finally, LST heavy liquid columns are used to separate quartz from any remaining minerals.

Pure quartz from each sample is then rinsed in 1% HF, massed, and ~15g of quartz per sample is spiked with ^{9}Be and ^{26}Al carriers of known concentrations and mass. Samples are dissolved in concentrated HF. Aliquots are separated at this point in case the samples need to be analyzed for aluminum.

The samples are then dried and fumed with $HClO_4$ to remove fluorides introduced by the HF. The samples are dried again and dissolved in HCl and ran through cation and anion columns. This purifies and separates Be via ion exchange chromatography. Next Be is precipitated using H_2O_2 and NH_3 and then oxidized to BeO at ~700 °C in a quartz crucible. Finally the samples are mixed with Nb metal and mounted to AMS targets and sent to the PRIME lab at Purdue University for AMS determination of ^{10}Be/^{9}Be ratios.

The measured isotope ratios are converted to ^{10}Be concentrations in quartz using the total Be in the samples and the sample weights. Production rates are scaled to the latitude and elevation of the sample site using the CRONUS-Earth Geometric Shielding Calculator (Balco et al., 2008).

Results

^{10}Be Exposure Ages of Boulders on Cascade Lake Moraines

To ease comparison with the results of the comprehensive study of Rood et al. (2011a), ages are reported (Table 1, Figure 8) using the Lal (1991)/ Stone (2000) time-dependent model with: no erosion, a preferred erosion rate of 0.6 m/Ma (Rood et al., 2011a), and a maximum erosion rate of 3.1 m/Ma (Small et al., 1997; Rood et al., 2011a). In reality, erosion rates are likely higher in the Tahoe region that experiences greater intensity forest fires (e.g. Burke and Birkeland, 1979) and receives more annual precipitation than farther to the south in the more arid Central Eastern Sierra where the majority of other cosmogenic studies have been completed. In modern times, South Lake Tahoe, CA receives an average of ~52 cm/yr of precipitation (NOAA, 2012), double that of Bridgeport, CA (~24 cm/yr), near several of the study sites from Rood et al. (2011a) (Figure 3).

Cosmogenic ages without erosion for the Tioga moraine range from 12.4-23.1 ka, and for the Tahoe moraine range from 14.5-113.4 ka (Table 1, Figure 8). With the preferred erosion rate of 0.6 m/Ma (Rood et al., 2011a), these ranges become 13.9-23.4 ka and 14.6-120.5 ka, for the Tioga and Tahoe moraines, respectively, and with the maximum erosion rate of 3.1 m/Ma these ranges become 14.3-24.6 ka and 15.1-173.3 ka, respectively.

Figure 8 graphically displays these results in two ways. The upper two plots show each individual sample plotted against its age with each of the varying erosion rates (error bars are for the 0.6 m/Ma erosion rate). On the upper-left Tioga plot, the blue bar shows the best estimate (mean of 7 samples omitting a young outlier) of the age of deposition with its error (standard deviation of the 7 samples), and on the upper-right Tahoe plot, the dashed line is the minimum age for the deposit based on the age of the oldest sample, CT-1. The lower two plots are cumulative probability density functions (PDFs) for each of the moraines produced by the methods outlined in Rood et al. (2011a): each sample is displayed as a Gaussian PDF with a mean of the age (with the 0.6 m/Ma erosion rate) and a 1σ standard deviation of the analytical error. Cumulative PDFs are displayed as a sum of the individual PDFs.

Sampl name	Latitude (DD)	Longitud (DD)	Altitud (m)	Thickn (cm)	Densi (g/cm	Shieldi factor	[Be-10] (atoms/	+/- (atoms/	Be standar	Minimum 0.0	m/Ma	+/-	Preferred 0.6	m/Ma	+/-	Maximum 3.1	m/Ma	+/-
Tahoe Footwall																		
CT-1	38.9298	-	2221	2	2.7	1	226408	40297	07KNS	113374		1017	120518		1152	173303		2586
CT-2	38.9300	-	2217	2	2.7	1	129668	40464	07KNS	64317		5941	66533		6362	78480		9007
CT-3	38.9303	-	2213	2	2.7	1	451899	33472	07KNS	22240		2528	22494		2586	23640		2861
CT-4	38.9301	-	2217	2	2.7	1	495417	25143	07KNS	24330		2431	24633		2492	26018		2787
Tioga Footwall																		
CT-5	38.9300	-	2218	2	2.7	1	454396	14081	07KNS	22289		2036	22544		2083	23695		2305
CT-6	38.9301	-	2214	2	2.7	1	427324	18990	07KNS	21010		2033	21235		2077	22253		2284
CT-7	38.9306	-	2209	2	2.7	1	410880	22778	07KNS	20265		2073	20476		2117	21418		2320
CT-8	38.9304	-	2206	2	2.7	1	415943	28695	07KNS	20558		2268	20772		2316	21745		2542
Tahoe Hangingwall																		
CT-9	38.9317	-	2124	2	2.7	1	118338	44866	07KNS	62439		5924	64486		6327	75654		8846
CT-10	38.9316	-	2134	2	2.7	1	162847	32999	07KNS	85844		7696	89809		8440	114278		1416
CT-11	38.9316	-	2132	4	2.7	1	461631	44616	07KNS	24401		3166	24705		3246	26099		3630
CT-12	38.9314	-	2135	1	2.7	1	282113	28712	07KNS	14478		1930	14584		1959	15053		2088
Tioga Hangingwall																		
CT-13	38.9323	-	2126	2	2.7	1	265453	9106	07KNS	13819		1276	13918		1294	14342		1375
CT-14	38.9327	-	2130	2	2.7	1	376066	22221	07KNS	19552		2040	19749		2081	20622		2273
CT-15	38.9329	-	2126	2	2.7	1	378789	12898	07KNS	19748		1824	19948		1861	20840		2034
CT-16	38.9341	-	2116	2.5	2.7	1	437984	15108	07KNS	23103		2139	23378		2191	24618		2434

able 1. ^{10}Be sample locations, concentrations, and exposure ages with varying erosion rates.

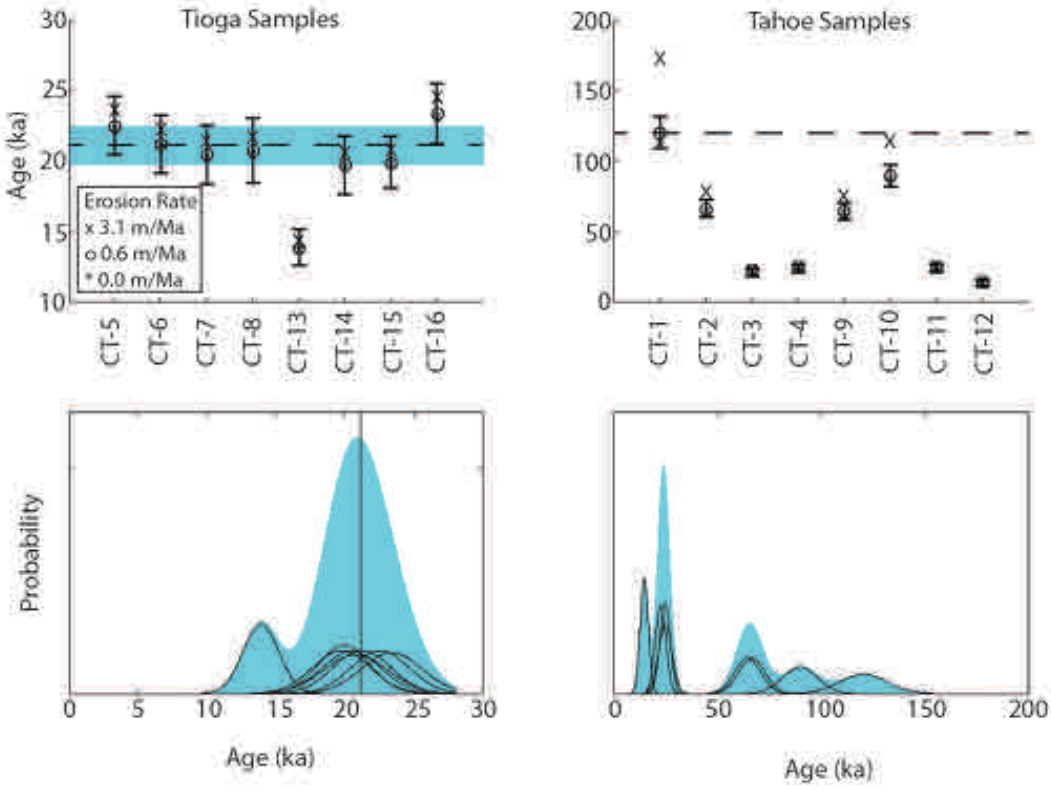

Figure 8 Plots of ages from the two surfaces with varying erosion rates (upper), and cumulative probability density functions (lower). Upper plots: asterisk symbols are with no erosion rate, circles and error bars are for preferred 0.6 m/Ma erosion, and x's are for the 3.1 m/Ma erosion rate. For the Tioga samples (upper left) the dashed horizontal line shows the mean and the cyan box shows the standard deviation of 7 samples, excluding CT-13. For the Tahoe samples (upper right), the dashed line is the minimum age of the deposit based on the oldest sample, CT-1. Lower plots: individual PDF's for each sample (black lines) and cumulative PDF's (cyan).

Discussion

Glacial History

The results from the Tioga deposit contain a single young outlier, and if excluded the remaining samples have a mean of 21.2 ± 1.2 ka, with the preferred 0.6 m/Ma erosion rate (Rood et al., 2011a) (Figure 8). This age is within the margin of error of the 18.8 ± 1.9 ka age that Rood et al. (2011a) measured from 12 Tioga moraines spanning the Sierra Nevada. Both of these ages correlate with MIS 2 (Figure 4).

The results from the Tahoe deposit are scattered from 14.6 ± 2.0 to 120.5 ± 11.5 ka (with the 0.6 m/Ma erosion rate) (Figure 8, Table 1). This scatter is interpreted to be the result of post-depositional processes (e.g. Wesnousky et al., 2016; Rood et al., 2011a; Phillips et al., 2009). Glacial boulder deposits do not contain significant cosmogenic

inheritance (e.g. Heyman et al., 2011), so the oldest age measured is here considered a minimum age of deposition.

This oldest measured 120.5 ± 11.5 ka age falls within the error of the 144 ± 14 ka age that Rood et al. (2011a) presented based on 30 measurements from 4 Tahoe moraines in the central-eastern Sierra Nevada, and correlates with MIS 6 (Figure 4). Considering that Rood et al. (2011a) found evidence for a two-stage Tioga-Tahoe glacial history in the Sierra Nevada (Figure 3), and nowhere did they find evidence for a MIS 4 glaciation, it follows that the double-crested moraines in the Tahoe Basin are from the same two Tioga and Tahoe stages as elsewhere in the Sierra, and not from a MIS 4, ~70 ka stage as Howle et al. (2012) proposed based on a single OSL age and a single cosmogenic age in the Tahoe basin (Figure 5). This demonstrates the importance of collecting large numbers of cosmogenic samples from older moraines, and as this oldest 120.5 ka age is still a minimum, perhaps if more samples were collected there would begin to be a cluster of ages more similar to Rood et al. (2011a)'s.

Slip rates of the West Tahoe Fault at Cascade Lake

As the projections of the moraines across the fault are not parallel, there is a wide range of possible vertical offsets: from 47-70 m for the Tahoe moraine and from 19-44 m for the Tioga moraine (Figure 6, Table 2), depending on whether the measurement is taken by comparing projections of the moraine surfaces at the toe or at the head of each scarp. Vertical separation rates are calculated by dividing these vertical offset measurements by the age of each moraine (Tioga: 21.2 ± 1.2 ka, Tahoe: 120.5 ± 11.5 ka), resulting in rates of 1.5 ± 0.7 mm/yr for the Tioga moraine, and 0.5 ± 0.1 mm/yr for the Tahoe moraine (Table 2).

Slip rates are calculated by dividing the vertical separation rate by the sine of the fault dip. A fault dip of 60° is assumed for the West Tahoe Fault based on estimates from trenches of the neighboring Genoa fault (Figure 2) (e.g. Ramelli et al., 1999), as well as Mohr-Coulomb failure criteria for normal faults (e.g. McCalpin, 2009). For the vertical separation rates of 1.5 ± 0.7 mm/yr (post-Tioga) and 0.5 ± 0.1 mm/yr (post-Tahoe), a 60° dipping normal fault geometry results in a slip rate of 1.7 ± 0.8 mm/yr (post-Tioga) and 0.6 ± 0.2 mm/yr (post-Tahoe). Uncertainty in the dip of the fault increases the uncertainty on these rates as shown by the varying fault dips in Table 2. Fault dips ranging from 50-70° result in slip rates of 1.7 +1.2/-0.8 mm/yr (post-Tioga) and 0.6 ± 0.2 mm/yr (post-Tahoe) (Table 2). Because exposure ages of glacial deposits are minimums, and especially so for older deposits, these should be considered maximum rates. Horizontal extension rates are calculated by dividing the vertical separation rate by the tangent of the fault dip, resulting in 0.9 ± 0.4 mm/yr (post-Tioga) and 0.3 ± 0.1 mm/yr (post-Tahoe).

		Age (ka)	Vertical separation (m)	Vertical Separation rate (mm/yr)	Extension fault dips 50	60	70	-Slip rate - fault dips 50	60	70
Tioga	min	20	19	0.8	0.7	0.5	0.3	1.1	1.0	0.9
	max	22.4	44	2.2	1.8	1.3	0.8	2.9	2.5	2.3
	mean	21.2	32	1.5	1.2	0.9	0.5	1.9	1.7	1.6
Taho	min	109	47	0.4	0.3	0.2	0.1	0.5	0.4	0.4
	max	130	70	0.6	0.5	0.4	0.2	0.8	0.7	0.7
	mean	120.5	59	0.5	0.4	0.3	0.2	0.6	0.6	0.5

Table 2. Summary of offset calculations: minimum, maximum, and average slip rates for variations in fault dip. Averaged rates in green, preferred in blue. Ages used are the maximum age from the Tahoe deposit, and the mean age (omitting a single outlier) from the Tioga deposit, with an erosion rate of 0.6 m/Ma.

Post-Tioga increase in slip rate of the West Tahoe Fault?

Regardless of how the scarp heights are measured (comparing toe to toe or head to head), the scarp in the Tioga surface is about half of the height of that in the Tahoe surface (~30 m vs. ~60 m) (Figure 6), and assuming that the faulted Tahoe moraine is at least six times the age of the Tioga moraine based on the ages that were measured (21.2 ka vs. 120.5 ka) (Figure 8), then at face value there is a large increase in slip rate in post-Tioga time. Figure 9 shows several possible slip rate histories through time.

The observed slip (solid black line on Figure 9) is derived from the two scarp heights for the faulted moraines and the trench data of Seitz (2015). As the Tahoe and Tioga surfaces are adjacent, it follows that the ~60 m total Tahoe displacement contains the same ~30 m displacement as the Tioga surface, and therefore immediately before Tioga time the scarp in the Tahoe surface should have been ~30 m high (60-30=30 m; Figure 9). The same approach can be taken with the 30 m of post-Tioga displacement and the post-10 ka ~3 m net displacement measured in a trench by Seitz (2015). This approach leads to three slip rates: a ~120-20 ka Tahoe-Tioga rate of ~0.3 mm/yr, a ~20 ka post-Tioga until 10 ka rate of ~2.5 mm/yr, and a post-10 ka rate of ~0.3 mm/yr (Figure 9). This results in an apparent over eight-fold increase in slip rate for a short time period following the Tioga glaciation. The modern geodetic extension rate of 1.1 ± 0.4 mm/yr (Bormann et al., 2016) is more similar to the post-Tioga average extension rate of 0.9 ± 0.4 mm/yr, than the post-Tahoe average rate, suggesting that the slip rate here may have increased following the Tioga glaciation.

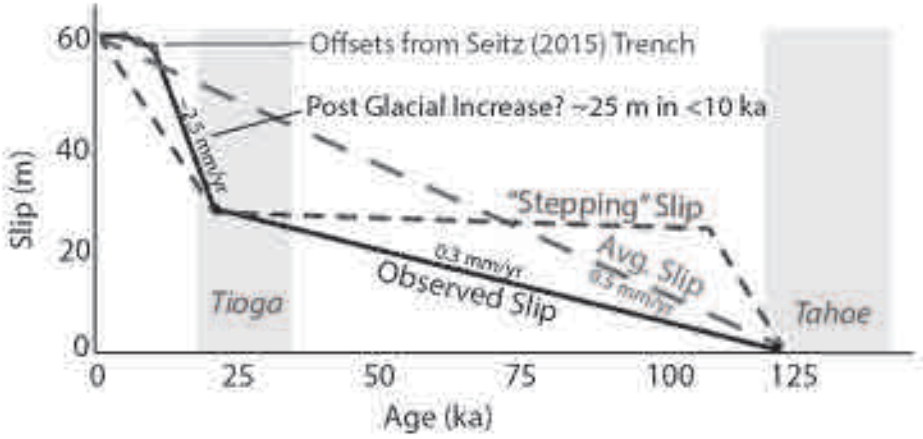

Figure 9 Slip vs. time for three different slip histories for the West Tahoe Fault based on: observations (solid dark line) from faulted moraines (black dots) and Seitz (2015)'s trench (gray dots); an average slip based on the height of the Tahoe moraine (long dashes); and a hypothetical "stepping slip" history based on the glacially-controlled slip rate model discussed in the text (short dashes).Grey bars indicate the approximate time spans of the Tioga and Tahoe glaciations.

If this apparent increase in slip rate is real, then it could be correlated with unloading of the footwall wall due to melting of the icecaps in the Sierra and unloading of the hanging wall due to the post-glacial decrease in the water level of Lake Tahoe (Birkeland, 1964, 1968). This phenomenon has been documented before where it has been shown that ~70% of the post-glacial slip on the Teton fault occurred shortly after the retreat of the MIS 2 Pinedale glaciation and before the oldest trenched earthquake circa 8 ka (Hampel et al., 2007). It has also been documented in Utah, where the drying of Lake Bonneville and deglaciation of the Wasatch Range coincides with a 2-8 fold increase in slip rate on the Wasatch Fault (Hetzel and Hampel, 2005). Following this model of rapid post-glacial/pluvial slip, it might be expected that there was a rapid increase in slip rate shortly after the Tahoe glaciation, which is only possible with the observed scarp heights if the inter-glacial slip rate is very low, resulting in a stepping pattern of slip rate through time that is closely tied to glaciations and climate (short dashed gray line on Figure 9).

However, as my 0.5 ± 0.1 mm/yr post-Tahoe vertical separation rate is both similar to previous estimates of ~0.3-0.8 mm/yr for the West Tahoe Fault (e.g. Howle et al., 2012; Dingler et al., 2009; Kent et al., 2005), and to rates measured for the Sierra Frontal Fault at Sonora Junction and Buckeye Creek (Figure 3), where slip rates have been steady over the 20-150 ka timescale (Rood et al., 2011b), We suggest that it is likely that the slip rate for the West Tahoe Fault has also been relatively constant, and this apparent change in slip rate is actually a result of a depositional or erosional process, and not a real change (average slip model on Figure 9). Perhaps most likely is that the Tioga moraine was draped over a preexisting fault scarp, and that a portion of the apparent offset is inherited from preexisting displacement and topography. This results in an apparent rather than real post-Tioga slip rate. If the post-Tahoe vertical separation rate is more accurate, then the ~21 ka Tioga scarp should be ~10 m tall, not 19-44 m as measured from profile (Figure 6). This expected 10 m displacement is similar to the

~10.5 m vertical offset measured in an offshore Tioga-aged fan delta (Dingler et al., 2009), and this rate could also produce the ~4 m scarps in post-Tioga deposits between Cascade Lake and Fallen Leaf Lake (Howle et al., 2012; Seitz, 2015) (Figure 5).

These hypotheses are not mutually exclusive: it is possible that there was some increase in slip rate following the deglaciations of the Sierra Nevada, and also that a part of the apparent slip on the Tioga moraine at Cascade Lake is a result of depositional process.

Seismic hazards for the Lake Tahoe Basin

Studies of empirical relations that correlate surface rupture/fault length with magnitude and displacement (e.g. Wells and Coppersmith, 1994; Wesnousky, 2008) show that a 45 km long rupture (based on the length of the West Tahoe Fault) is typically associated with an M6.9 earthquake for a normal fault (Wells and Coppersmith, 1994). Using the correlation between maximum and average surface displacements and surface rupture length from Wesnousky (2008), for a 45 km long normal fault, there is an average surface slip of 1.3 m and a maximum surface slip of 4 m. This average surface slip is similar to the average of ~1.1 m for the three events that Seitz (2015) observed in a trench of the West Tahoe Fault. Dividing the magnitude of the average slip by my (post-Tahoe) slip rate of 0.6 mm/yr allows for a return time of 2.2 ka. If the likely unrealistic post-Tioga slip rate of 1.8 mm/yr is used, this return time becomes 700 years.

Seitz's (2015) trench results show an average return time over the last 10 ka of ~3.3 ka/event, which is higher than my 2.2 ka/event estimate of recurrence, however, my estimate is more similar to the actual return times (~1.8 and ~1.7 kyr) between these trenched events. These estimates of recurrence are also similar to those of Maloney et al. (2013), who postulate a return time of 3-4 kyr between large earthquakes along the West Tahoe Fault based on the age of presumed seismically triggered submarine slide deposits that correlate in age across Fallen Leaf Lake, Cascade Lake, and Lake Tahoe. However, considering that the most recent earthquake on the West Tahoe Fault occurred at ~5.5 ka (Seitz, 2015; Maloney et al., 2013), the return time is highly variable. Furthermore, since this most recent earthquake occurred at ~5.5 ka, exceeding all of these estimates of return time, it is likely that the West Tahoe Fault is in the late stages of its strain accumulation cycle. Considering all of the above, an average return time of 2-4 ka for ~M7 events on the West Tahoe Fault is reasonable.

Conclusion

Interpretation of ^{10}Be ages on moraines mapped as Tioga and Tahoe in age at Cascade Lake indicates that they were deposited during Stages II and VI of the oxygen isotope record, respectively. The Tioga and Tahoe moraines exhibit progressively greater vertical offsets of 32 and 59 meters due to displacement by the West Tahoe Fault. Dividing these offsets by the minimum ages of the moraines yields bounds on the vertical fault slip rate of 1.5 ± 0.7 and 0.5 ± 0.1 mm/yr since emplacement of the Tioga and Tahoe moraines, respectively. The results at face value imply a rapid increase in slip rate with time. Because the post-Tioga rate is higher than previous estimates, and Rood et al. (2011b) show that elsewhere in the region slip rates have been relatively

constant for this time period, we suspect that the younger faster rate does not truly reflect the fault slip rate. In this respect, the vertical fault slip rate of the West Tahoe fault is here estimated to be 0.5 ± 0.1 mm/yr.

References

Angster, S., Wesnousky, S., Huang, W., Kent, G., Nakata, T., Goto, H., 2016. Application of UAV Photography to Refining the Slip Rate on the Pyramid Lake Fault Zone, Nevada. Bull. Seismol. Soc. Am. 106, 785–798. doi:10.1785/0120150144

Balco, G., Stone, J.O., Lifton, N.A., Dunai, T.J., 2008. A complete and easily accessible means of calculating surface exposure ages or erosion rates from 10Be and 26Al measurements. Quat. Geochronol. 3, 174–195. doi:10.1016/j.quageo.2007.12.001

Beanland, S., Clark, M.M., 1994. The Owens Valley Fault Zone, Eastern California, and Surface Faulting Associated with the 1872 Earthquake (U.S. Geological Survey Bulletin No. 1982). U.S. Geological Survey.

Benn, D.I., Owen, L.A., Finkel, R.C., Clemmens, S., 2006. Pleistocene lake outburst floods and fan formation along the eastern Sierra Nevada, California: implications for the interpretation of intermontane lacustrine records. Quat. Sci. Rev. 25, 2729–2748. doi:10.1016/j.quascirev.2006.02.018

Bennett, R.A., Wernicke, B.P., Niemi, N.A., Friedrich, A.M., Davis, J.L., 2003. Contemporary strain rates in the northern Basin and Range province from GPS data. Tectonics 22, n/a-n/a. doi:10.1029/2001TC001355

Bierman, P., Gillespie, A., 1991. Range fires: A significant factor in exposure-age determination and geomorphic surface evolution. Geology 19, 641–644.

Birkeland, P.W., 1968. Mean Velocities and Boulder Transport During Tahoe–Age Floods of the Truckee River, California–Nevada. Geol. Soc. Am. Bull. 79, 137–142.

Birkeland, P.W., 1964. Pleistocene Glaciation of the Northern Sierra Nevada, North of Lake Tahoe, California.

Birkeland, P.W., Burke, R.M., 1979. The problem of correlation with the Tahoe-Truckee area, in: Field Guide to Relative Dating Methods Applied to Glacial Deposits in the Third and Fourth Recesses and along the Easter Sierra Nevada, California with Supplementary Notes on Other Sierra Nevada Localities. p. 131.

Birman, J.H., 1964. Glacial geology across the crest of the Sierra Nevada, California. Geol. Soc. Am. Spec. Pap. 75, 80.

Blackwelder, E., 1931. Pleistocene glaciation in the Sierra Nevada and basin ranges. Geol. Soc. Am. Bull. 42, 865–922.

Bormann, J.M., Hammond, W.C., Kreemer, C., Blewitt, G., 2016. Accommodation of missing shear strain in the Central Walker Lane, western North America: Constraints from dense GPS measurements. Earth Planet. Sci. Lett. 440, 169–177. doi:10.1016/j.epsl.2016.01.015

Brothers, D.S., Kent, G.M., Driscoll, N.W., Smith, S.B., Karlin, R., Dingler, J.A., Harding, A.J., Seitz, G.G., Babcock, J.M., 2009. New Constraints on Deformation, Slip

Rate, and Timing of the Most Recent Earthquake on the West Tahoe-Dollar Point Fault, Lake Tahoe Basin, California. Bull. Seismol. Soc. Am. 99, 499–519. doi:10.1785/0120080135

Burke, R.M., Birkeland, P.W., 1979. Reevaluation of Multiparameter Relative Dating Techniques and Their Application to the Glacial Sequence Along the Eastern Escarpment of the Sierra Nevada. Quat. Res. 11, 21–51.

Bursik, M.L., Gillespie, A.R., 1993. Late Pleistocene Glaciation of Mono Basin, California. Quat. Res. 39, 24–35.

Clark, M.M., 1967. Pleistocene glaciation of the upper West Walker drainage, Sierra Nevada, California (Dissertation). Stanford University, Stanford.

Dalrymple, G.., 1964. Cenozoic chronology of the Sierra Nevada, California. Calif Univ Publ Geol Sci 47.

Dalrymple, G.B., Burke, R.M., Birkeland, P.W., 1982. Concerning K-Ar Dating of a Basalt Flow from the Tahoe-Tioga Interglaciation, Sawmill Canyon, Southeastern Sierra Nevada, California. Quat. Res. 17, 120–122.

Dingler, J., Kent, G., Babcock, J., Harding, A., Seitz, G., Karlin, B., Goldman, C., 2009. A high-resolution seismic CHIRP investigation of active normal faulting across Lake Tahoe Basin, California-Nevada.

Dixon, T.H., Miller, M., Farina, F., Wang, H., Johnson, D., 2000. Present-day motion of the Sierra Nevada block and some tectonic implications for the Basin and Range province, North American Cordillera. Tectonics 19, 1–24.

Freymueller, J.T., Murray, M.H., Segall, P., Castillo, D., 1999. Kinematics of the Pacific-North America plate boundary zone, northern California. J. Geophys. Res. 104, 7419–7441.

Fullerton, D.S., 1986. Chronology and correlation of glacial deposits in the Sierra Nevada, California. Quat. Sci. Rev. 5, 161–169. doi:10.1016/0277-3791(86)90181-2

Gillespie, A.R., 1991. Testing a New Climatic Interpretation for the Tahoe Glaciation, in: Geomorphology/Paleoclimatology. pp. 383–398.

Gillespie, A.R., 1982. Quaternary Glaciation and Tectonism in the Southeastern Sierra Nevada, Inyo County, California (Ph.D.). California Institute of Technology, Pasadena, California.

Gillespie, A.R., Clark, D.H., 2011. Chapter 34 - Glaciations of the Sierra Nevada, California, USA, in: Jürgen Ehlers, P.L.G. and P.D.H. (Ed.), Developments in Quaternary Sciences, Quaternary Glaciations - Extent and Chronology A Closer Look. Elsevier, pp. 447–462.

Gold, R.D., Briggs, R.W., Personius, S.F., Crone, A.J., Mahan, S.A., Angster, S.J., 2014. Latest Quaternary paleoseismology and evidence of distributed dextral shear along the Mohawk Valley fault zone, northern Walker Lane, California: Paleoseismology Mohawk Valley fault zone. J. Geophys. Res. Solid Earth 119, 5014–5032. doi:10.1002/2014JB010987

Gosse, J.C., Phillips, F.M., 2001. Terrestrial in situ cosmogenic nuclides: theory and application. Quat. Sci. Rev. 20, 1475–1560.

Hammond, W.C., Blewitt, G., Kreemer, C., 2011. Block modeling of crustal deformation of the northern Walker Lane and Basin and Range from GPS velocities. J. Geophys. Res. 116. doi:10.1029/2010JB007817

Hampel, A., Hetzel, R., Densmore, A.L., 2007. Postglacial slip-rate increase on the Teton normal fault, northern Basin and Range Province, caused by melting of the

Yellowstone ice cap and deglaciation of the Teton Range? Geology 35, 1107–1110.

Hetzel, R., Hampel, A., 2005. Slip rate variations on normal faults during glacial-interglacial changes in surface loads. Nature 435, 81–84.

Heyman, J., Stroeven, A.P., Harbor, J.M., Caffee, M.W., 2011. Too young or too old: Evaluating cosmogenic exposure dating based on an analysis of compiled boulder exposure ages. Earth Planet. Sci. Lett. 302, 71–80. doi:10.1016/j.epsl.2010.11.040

Howle, J.F., Bawden, G.W., Schweickert, R.A., Finkel, R.C., Hunter, L.E., Rose, R.S., von Twistern, B., 2012. Airborne LiDAR analysis and geochronology of faulted glacial moraines in the Tahoe-Sierra frontal fault zone reveal substantial seismic hazards in the Lake Tahoe region, California-Nevada, USA. Geol. Soc. Am. Bull. 124, 1087–1101.

Hunter, L.E., Howle, J.F., Rose, R.S., Bawden, G.W., 2011. LiDAR-Assisted Identification of an Active Fault near Truckee, California. Bull. Seismol. Soc. Am. 101, 1162–1181. doi:10.1785/0120090261

Kent, G.M., Babcock, J.M., Driscoll, N.W., Harding, A.J., Dingler, J.A., Seitz, G.G., Gardner, J.V., Mayer, L.A., Goldman, C.R., Heyvaert, A.C., Richards, R.C., Karlin, R., Morgan, C.W., Gayes, P.T., Owen, L.A., 2005. 60 k.y. record of extension across the western boundary of the Basin and Range province: Estimate of slip rates from offset shoreline terraces and a catastrophic slide beneath Lake Tahoe. Geology 33, 365–368. doi:10.1130/G21230.1

Kohl, C.P., Nishiizumi, K., 1992. Chemical isolation of quartz for measurement of in-situ-produced cosmogenic nuclides. Geochim. Cosmochim. Acta.

Lal, D., 1991. Cosmic ray labeling of erosion surfaces: in situ nuclide production rates and erosion models. Earth Planet. Sci. Lett. 104, 424–439.

Maloney, J.M., Noble, P.J., Driscoll, N.W., Kent, G.M., Smith, S.B., Schmauder, G.C., Babcock, J.M., Baskin, R.L., Karlin, R., Kell, A.M., Seitz, G.G., Zimmerman, S., Kleppe, J.A., 2013. Paleoseismic history of the Fallen Leaf segment of the West Tahoe-Dollar Point fault reconstructed from slide deposits in the Lake Tahoe Basin, California-Nevada. Geosphere 9, 1065–1090. doi:10.1130/GES00877.1

Martinson, D.G., Pisias, N.G., Hays, J.D., Imbrie, J., Moore, T.C., Shackleton, N.J., 1987. Age dating and the orbital theory of the ice ages: development of a high-resolution 0 to 300,000-year chronostratigraphy. Quat. Res. 27, 1–29.

McCalpin, J., 2009. Paleoseismology, 2nd ed. Academic Press.

McCaughey, J.W., 2003. Pleistocene glaciation of the southwest Tahoe basin: Sierra Nevada, California (M.S.). University of Nevada, Reno, United States -- Nevada.

NOAA, 2012. 1981-2010 Climate Normals.

Owen, L.A., Finkel, R.C., Caffee, M.W., Gualtieri, L., 2002. Timing of multiple late Quaternary glaciations in the Hunza Valley, Karakoram Mountains, northern Pakistan: defined by cosmogenic radionuclide dating of moraines. Geol. Soc. Am. Bull. 114, 593–604.

Phillips, F.M., Zreda, M., Benson, L.V., Plummer, M.A., Elmore, D., Sharma, P., 1996. Chronology for Fluctuations in Late Pleistocene Sierra Nevada Glaciers and Lakes. Science 274, 749.

Phillips, F.M., Zreda, M., Plummer, M.A., Elmore, D., Clark, D.H., 2009. Glacial geology and chronology of Bishop Creek and vicinity, eastern Sierra Nevada, California. Geol. Soc. Am. Bull. 121, 1013–1033. doi:10.1130/B26271.1

Phillips, F.M., Zreda, M., Smith, S.S., Elmore, D., Kubik, P.W., Sharma, P., 1990. Cosmogenic Chlorine-36 Chronology for Glacial Deposits at Bloody Canyon, Eastern Sierra Nevada. Science 248, 1529.

Pisias, N.G., Martinson, D.G., Moore, T.C., Shackleton, N.J., Prell, W., Hays, J., Boden, G., 1984. High resolution stratigraphic correlation of benthic oxygen isotopic records spanning the last 300,000 years. Mar. Geol. 56, 119–136.

Putkonen, J., O'Neal, M., 2006. Degradation of unconsolidated Quaternary landforms in the western North America. Geomorphology 75, 408–419. doi:10.1016/j.geomorph.2005.07.024

Putkonen, J., Swanson, T., 2003. Accuracy of cosmogenic ages for moraines. Quat. Res. 59, 255–261. doi:10.1016/S0033-5894(03)00006-1

Putnam, A.E., 2016. Age of the Tioga glaciation at Convict Lake, personal communication.

Putnam, W.C., 1960. Faulting and Pleistocene glaciation in the east-central Sierra Nevada of California, U.S.A. Nord. Intern. Geol Cong 21st Sess 270–274.

Putnam, W.C., 1949. Quaternary geology of the June Lake district, California. Geol Soc Am. Bull 60, 1281–1302.

Ramelli, A.R., Bell, J.W., dePolo, C.M., Yount, J.C., 1999. Large-magnitude, late Holocene earthquakes on the Genoa fault, west-central Nevada and eastern California. Bull. Seismol. Soc. Am. 89, 1458–1472.

Rood, D.H., Burbank, D.W., Finkel, R.C., 2011a. Chronology of glaciations in the Sierra Nevada, California, from 10Be surface exposure dating. Quat. Sci. Rev. 30, 646–661. doi:10.1016/j.quascirev.2010.12.001

Rood, D.H., Burbank, D.W., Finkel, R.C., 2011b. Spatiotemporal patterns of fault slip rates across the Central Sierra Nevada frontal fault zone. Earth Planet. Sci. Lett. 301, 457–468. doi:10.1016/j.epsl.2010.11.006

Saucedo, G.J., 2005. Geologic Map of the Lake Tahoe Basin.

Schaefer, J., 2006. Near-Synchronous Interhemispheric Termination of the Last Glacial Maximum in Mid-Latitudes. Science 312, 1508–1510. doi:10.1126/science.1125684

Schweickert, R.A., Lahren, M.M., Smith, K.D., Howle, J.F., Ichinose, G., 2004. Transtensional deformation in the Lake Tahoe region, California and Nevada, USA. Tectonophysics, Continental Margins of the Pacific Rim 392, 303–323. doi:10.1016/j.tecto.2004.04.019

Seitz, G., 2015. The West Tahoe Fault.

Sharp, R.P., 1972. Pleistocene Glaciation, Bridgeport Basin, California. Geol. Soc. Am. Bull. 83, 2233–2260.

Sharp, R.P., Birman, J.H., 1963. Additions to classical sequence of Pleistocene glaciations, Sierra Nevada, California. Geol. Soc. Am. Bull. 74, 1079–1086.

Small, E.E., Anderson, R.S., Repka, J.L., Finkel, R., 1997. Erosion rates of alpine bedrock summit surfaces deduced from in situ 10Be and 26Al. Earth Planet. Sci. Lett. 150, 413–425. doi:10.1016/S0012-821X(97)00092-7

Stone, J.O., 2000. Air pressure and cosmogenic isotope production. J. Geophys. Res. 105, 23,753-23,759.

Swan, F.H.I., Schwartz, D., Cluff, L.S., 1980. Recurrence of moderate to large magnitude earthquakes produced by surface faulting on the Wasatch fault zone, Utah. Bull. Seismol. Soc. Am. 70, 1431–1462.

Thatcher, W., Foulger, G.R., Julian, B.R., Svarc, J., Quilty, E., Bawden, G.W., 1999. Present-Day Deformation Across the Basin and Range Province, Western United States. Science 283, 1714–1717.

Unruh, J., Humphrey, J., Barron, A., 2003. Transtensional model for the Sierra Nevada frontal fault system, eastern California. Geology 31, 327–330.

Watershed Sciences, 2011. Lidar Remote Sensing Lake Tahoe Watershed, California/Nevada.

Wells, D.L., Coppersmith, K.J., 1994. New empirical relationships among magnitude, rupture length, rupture width, rupture area, and surface displacement. Bull. Seismol. Soc. Am. 84, 974–1002.

Wesnousky, S.G., 2008. Displacement and Geometrical Characteristics of Earthquake Surface Ruptures: Issues and Implications for Seismic-Hazard Analysis and the Process of Earthquake Rupture. Bull. Seismol. Soc. Am. 98, 1609–1632. doi:10.1785/0120070111

Wesnousky, S.G., 2005. Active faulting in the Walker Lane. Tectonics 24, n/a-n/a. doi:10.1029/2004TC001645

Wesnousky, S.G., Bormann, J.M., Kreemer, C., Hammond, W.C., Brune, J.N., 2012. Neotectonics, geodesy, and seismic hazard in the Northern Walker Lane of Western North America: Thirty kilometers of crustal shear and no strike-slip? Earth Planet. Sci. Lett. 329–330, 133–140. doi:10.1016/j.epsl.2012.02.018

Wesnousky, S.G., Briggs, R.W., Caffee, M.W., Ryerson, F.J., Finkel, R.C., Owen, L.A., 2016. Terrestrial cosmogenic surface exposure dating of glacial and associated landforms in the Ruby Mountains-East Humboldt Range of central Nevada and along the northeastern flank of the Sierra Nevada. Geomorphology 268, 72–81. doi:10.1016/j.geomorph.2016.04.027

Zreda, M., Phillips, F.M., Elmore, D., 1994. Cosmogenic 36Cl accumulation in unstable landforms 2. Simulations and measurments on eroding moraines. Water Resour. Res. 30, 3127–3136.

Supplemental S1: Photos of Sampled Boulders

CT-1

CT-2

CT-3

CT-4

CT-5

CT-6

CT-7

CT-8

CT-9

CT-10

CT-11

CT-12

CT-13

CT-14

CT-15

CT-16